www.czasopisma.pan.pl PAN www.journals.pan.pl

ARCHIVES of FOUNDRY ENGINEERING

ISSN (2299-2944)
Volume 2023
Issue 2/2023

29 – 34

10.24425/afe.2023.144292

5/2

Published quarterly as the organ of the Foundry Commission of the Polish Academy of Sciences

Precipitation of Sigma and Chi Phases in Cast Standard Duplex Stainless Steel

M. Myška *, P. Bořil, V. Krutiš, V. Kaňa, A. Záděra
Brno University of Technology, Czech Republic
* Corresponding author: Email address: Martin.Myska@vutbr.cz

Received 14.11.2022; accepted in revised form 25.01.2023; available online 28.04.2023

Abstract

This work deals with the problem of intermetallic phases in cast standard duplex steel ASTM A890 Gr 4A (generally known as 2205). The investigated steel was subjected to isothermal heat treatment in the range from 595 °C to 900 °C and in the duration from 15 minutes to 245 hours, and was also investigated in terms of anisothermal (natural) cooling after casting into the mould. The precipitation starts at grain boundaries with a consistent ferrite transformation. The work is focused on the precipitation of the sigma phase (σ) and the chi phase (χ). Examination of the microstructure was conducted using light and scanning electron microscopy. Their statistical analysis was carried out using the results of the investigations of precipitation processes in the microstructure, both within the grains and at the grain boundaries. To illustrate this impact, the surface area of precipitates was evaluated. The percentage of these intermetallic phases was calculated by measuring their area using a computer image analysis system. Based on their observations, a combined time-temperature transformation (TTT) diagram with continuous cooling transformation (CCT) curves was created.

Keywords: Precipitation, Cast duplex steel, Intermetallics, Sigma phase, Chi phase

1. Introduction

Duplex steels are generally considered to be steels with a two-phase structure. Duplex steels can have a combination of austenite, martensite and ferrite phases. Duplex stainless steels (DSS) are considered in this work as stainless chromium-nickel steels with an austenitic-ferritic structure.

The proportion of ferrite and austenite in duplex steel depends mainly on the chemical composition. It is generally known which elements positively affect the formation of austenite and which ones affect the formation of ferrite. At the same time, the elements in those phases have greater solubility [1, 2]:

- Austenite stabilising elements: Ni, C, N, Mn, Co, Cu,
- Ferrite stabilising elements: Cr, Mo, Si, Nb, Ti, Al, W, V, Ta.

The quality of duplex steel is influenced by the properties of individual structural elements of austenite and ferrite and their ratio, size and distribution. However, the morphology of oxide inclusions and various types of precipitates is unacceptable, especially in terms of corrosion resistance, since duplex steels are primarily used in a corrosive environment.

One of the parameters by which steels are specified is corrosion resistance using equations based on the chemical composition of the alloy. Commonly used is the Pitting Resistance Equivalent Number (PREN) (Eq. (1)), or the more recent MARC (Measure of Alloying for Resistance to Corrosion) equation, which is valid for super austenites and additionally considers C, Mn and Ni. According to the increasing content of alloying elements and the PREN value, duplex austenitic-ferritic steels are divided in ascending order into lean, standard, super and hyper duplex. [3, 4].

$$PREN = \%Cr + 3.3 \cdot \left(\%Mo + \frac{\%W}{2} \right) + 16 \cdot \%N \quad (1)$$

Table 1.
The nominal chemical composition in wt.% of ASTM A890 Gr 4A steel and the chemical composition in wt.% of the duplex steel used in this study

		C	Cr	Ni	Mo	Mn	Si	N	P	S	Cu	Al	PREN
Standard	**Min**	-	21.00	4.50	2.50	-	-	0.10	-	-	-	-	30.9
	Max	0.030	23.50	6.50	3.50	1.50	1.00	0.30	0.04	0.02	1.00	-	39.9
The first trial (TTT diagram)		0.028	22.89	5.05	2.97	0.93	0.41	0.19	0.02	<0.15	0.06	0.021	35.7
The second trial (cast condition)		0.027	22.69	4.93	3.10	0.88	0.35	0.22	<0.005	<0.15	0.05	0.019	36.4

These are the main criteria that describe duplex steel as a final product, but a problem arises from the point of view of the production of this steel by casting. This problem is caused by intermetallic particles that form at higher temperatures or during the cooling of the casting in the mould and cause degradation of the mechanical properties. Degradation of the mechanical properties can lead to a failure of the coherence of the casting, such as cracks and hot tears.

In general, publications deal with the impact of intermetallics in duplex steels from the point of view of erosion and corrosion [5,6], wear [7-9], welding [10], thermodynamic and kinetic calculations [11, 12], numerical modelling [13], mechanical properties [14], in connection with radioactivity [15], precipitation and phase analysis, where applicable, the goals of the publications are intertwined. However, duplex steels have a wide spectrum and ranges of elements that significantly influence the behaviour of precipitates, where the main criterion describing precipitation is the isothermal TTT diagram. From the point of view of the behaviour of the precipitates, it is important whether the metal is wrought [16,17] or cast or welded. For this reason, a custom TTT diagram of cast Gr 4A steel was created for verification and compared with the structure of continuously cooled Gr 4A steel of nearly the same chemical composition in the as-cast condition.

2. Material for research

The standard duplex steel ASTM A890 Gr4A was chosen for the work, and this steel was selected as the most typical representative of the standard duplex steel. This steel has the most potential for producing duplex steel castings. This grade is similar in chemical composition to UNS 31803/32205, AISI 318 LN, SAF 2205TM, DIN / EN 1.4462, or only 2205. Norm ASTM A890 is intended for castings of austenitic-ferritic duplex steels. The chemical composition according to this standard is given in Table 1. The table describes two trials with nearly the same chemical composition, which should not affect the experiment. The first trial was performed to obtain material for the compilation of the TTT diagram and was cast into a 60 mm Y block. The second trial was performed to obtain data on how the natural cooling rate of the casting in the mould affects the precipitation of the intermetallic phases and thus the mechanical properties. The cooling rate was varied by the wall thickness of the Y blocks (25, 50, 75 and 100 mm) and type S thermocouples were placed in the moulds to verify the cooling rate of the metal. The steel was melted on a vacuum induction furnace with a neutral lining and with the help of a vacuum process. The examined duplex steel has a PREN value of 35.7 and 36.4, ranking it among the standard duplex steel.

3. Experimental Methods and Theory

The investigated material from the first trial was freed of all undesired intermetallic particles by solution annealing at 1150 °C. It was verified that only austenite γ and δ ferrite were present in the matrix, which was essential for the experimental results. Small samples of the solution-treated steel were isothermally heat-treated and subsequently cooled in water, which led to the precipitation of secondary phases and their stabilisation. Ageing of Gr 4A steel leads to the precipitation of secondary phases in the δ ferrite grains and at the grain boundaries of γ/δ. During the initial ageing period, visible precipitation occurs in the test steel, intensifying with increasing ageing time and temperature. Unfortunately, the first precipitates of the secondary phases are not evenly distributed in the volume of the sample, which complicates the evaluation.

Ageing time ranged from 15 minutes for very early precipitates at high temperatures to 245 hours for lower temperatures where precipitation is slower. Ageing temperatures ranged from 595 °C to 900 °C. These times and temperatures are given in Table 2.

Table 2.
Performed ageing times and ageing temperatures

Temp.	Soak Time (hours)										
595 °C	1	2	5	10	24	49	72	96	168	245	
650 °C	1	2	5	10	24	50	100	150			
700 °C	1	2	4	6	8	10	20	40	60	80	150
800 °C	1/4	2/4	3/4	1	2	5	10	24	50		
900 °C	1/4	2/4	3/4	1	2	5	10	24	50		

Before the actual measurement on scanning electron microscope (SEM) images, specific metallographic samples were selected based on light microscope (LM) observations. The samples were etched using Beraha II reagent. The quantitative analysis of the precipitates was performed using the ImageJ computer image analysis system based on microstructure images obtained with a LM and a SEM at 2000× 1000×, 500× and 100× magnification, and the magnification differed according to the particle size. The ImageJ was calibrated to the scale bar on the microstructure images. Images were cropped to erase the image information, which would compromise the analysis. An example workflow after thresholding used during the image analysis to extract the analysed χ-phase precipitates is shown in Fig. 1.

Change in microstructure at these isothermal annealing temperatures is mainly reflected in δ ferrite, which is transformed into phases such as sigma phase (σ), chi phase (χ), chromium carbides ($M_{23}C_6$), chromium nitrides (Cr_2N), Laves phase (Fe_2W), secondary austenite (γ_2) and Widmanstätten austenite (γ_w). This work is focused mainly on the precipitation of the σ-phase and the χ-phase.

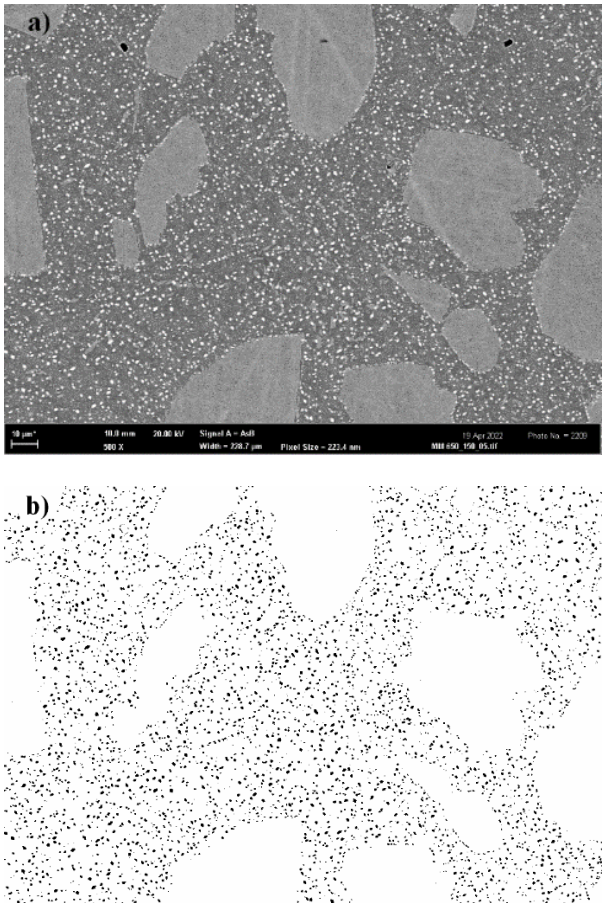

Fig. 1. Microstructure of the Gr 4A steel after 150 h of ageing at 650 °C (magnification 500x, bar 10 µm): a) original SEM image, b) thresholded image

The χ-phase occurs in duplex steel to a much lesser extent than the σ-phase. The χ-phase occurs only in Fe-Cr-Mo steels with a minimum molybdenum content of 2 wt.%. Compared to the σ-phase, the χ-phase is richer in molybdenum and poorer in chromium, highlighting the χ-phase significantly brighter using a scanning electron microscope. Since the χ-phase cannot be clearly distinguished from the σ-phase on an LM and is usually precipitated as small fine particles, the use of a SEM is recommended for easy analysis of the particles [18-20].

The σ-phase is based on Fe-Cr-Mo precipitates and occurs in austenitic, ferritic and austenitic-ferritic duplex steels. The precipitation starts at the γ/δ phase interface and increases towards the ferritic grain. When the σ-phase grows to δ ferrite, the ferrite stabilisers are depleted out of the ferritic matrix, and the δ ferrite is converted to the secondary austenite γ_2. This reaction can be described as a eutectoid transformation: $\delta \rightarrow \sigma + \gamma_2$. Typically, the σ-phase is recognisable with a coral morphology, and increasing temperature makes it larger and more compact. According to various studies, the fastest precipitation rate is around 800 °C, and the precipitation is additionally supported by Cu [8, 21, 22].

4. Compilation of the TTT diagram

The different ageing temperatures from 595 °C to 900 °C had a significant effect on the size and distribution of χ-phase and σ-phase precipitates (Fig. 1 and 2) in Gr 4A steel.

The χ-phase increases in size and precipitates faster with higher ageing temperatures, as shown for example in the histograms (Fig. 3 and 4) for two different ageing temperatures from 650 and 700 °C. Here in these two histograms, we can see that the largest χ-phase particle after 150 hours and at 650 °C has a size of 2.8 µm^2, while after the same time at 700 °C the size grows up to 8 µm^2, which is almost three times larger. The average size of the χ-phase is increasing from 0,1 µm^2 at 595 °C to 16 µm^2 at 900 °C but their number decreases as the ageing temperature rises. Table 3. summarises the main information regarding the χ-phase on the total area of the particles, their distribution, and the average and maximum size.

Table 3.
Summary of the χ-phase analysis; distribution, surface share, average size and maximum size

Ageing temp. [°C]	Ageing time [h]	Particles per µm^2 [µm^{-2}]	Surface share [%]	Average size [µm^2]	Maximum size [µm^2]
595	72	0.5	3.35	0.135	0.634
	168	0.67	3.74	0.111	0.698
	245	0.8	4.56	0.115	0.477
650	10	0.056	0.32	0.114	0.586
	150	0.126	2.93	0.467	2.633
700	80	0.059	1.93	0.651	7.920
	150	0.053	1.76	0.662	6.493
800	0.5	0.001	0.02	0.188	1.223
	10	0.059	1.68	1.266	12.726
	50	0.001	0.57	7.682	83.235
900	0.5	0.001	0.02	0.703	2.558
	10	0.002	0.15	5.702	40.356
	50	0.0003	0.04	15.934	64.318

The χ-phase and the σ-phase commonly occur together, our observations confirm the precipitation of the χ-phase earlier than the σ-phase. On our samples at ageing temperatures of 595 °C, precipitation of the χ-phase occurs after 10 hours, and the σ-phase was not found. At ageing temperatures of 650 °C, the χ-phase is visible after 5 hours and the σ-phase after 24 hours. At ageing temperatures of 700 °C, precipitation of the χ-phase begins after 2 hours and the σ-phase after 4 hours. At ageing temperatures of 800 and 900 °C, χ-phase and σ-phase precipitate before 30 minutes of ageing. However, the σ-phase on the sample aged at 800 °C after 50 hours shows the termination of the growth of precipitates, where almost all δ ferrite has been consumed, which confirms previous studies. At ageing temperatures from 700 °C to 900 °C, the χ -phase already begins to coarsen after a certain time, but at the same time it also dissolves in favour of the σ-phase and thus its decrease in the volume of the structure. This property is most noticeable at an ageing temperature of 800 °C. The compiled TTT diagram is shown in Fig. 5.

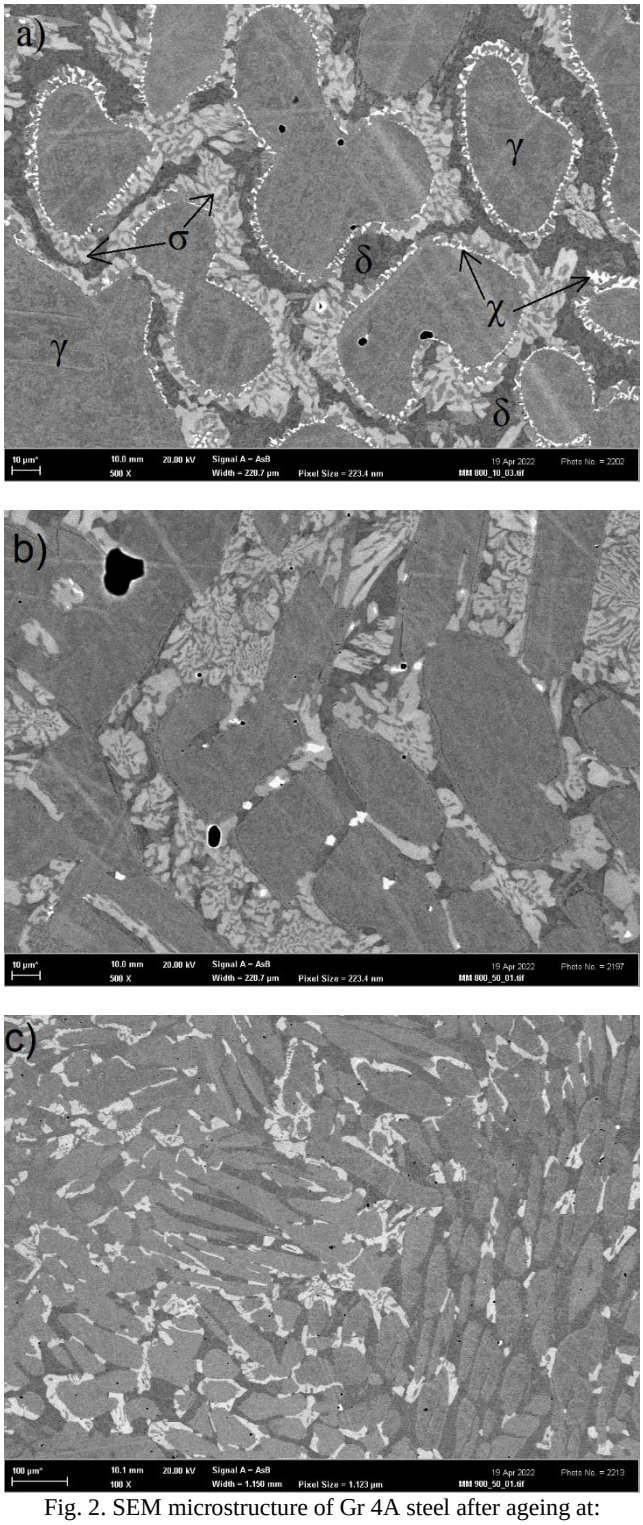

Fig. 2. SEM microstructure of Gr 4A steel after ageing at:
(a) 800 °C/10 h (magnification 500x, bar 10 µm),
(b) 800 °C/50 h (magnification 500x, bar 10 µm),
(c) 900 °C/50 h (magnification 100x, bar 100 µm)

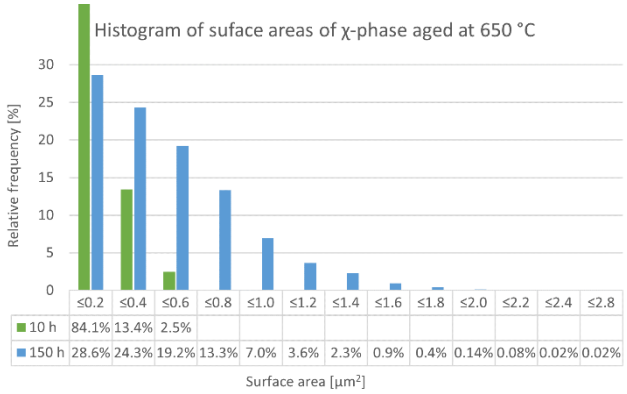

	≤0.2	≤0.4	≤0.6	≤0.8	≤1.0	≤1.2	≤1.4	≤1.6	≤1.8	≤2.0	≤2.2	≤2.4	≤2.8
10 h	84.1%	13.4%	2.5%										
150 h	28.6%	24.3%	19.2%	13.3%	7.0%	3.6%	2.3%	0.9%	0.4%	0.14%	0.08%	0.02%	0.02%

Fig. 3. Histogram of the surface area of χ-phase after ageing at 650 °C at different times in Gr 4A steel

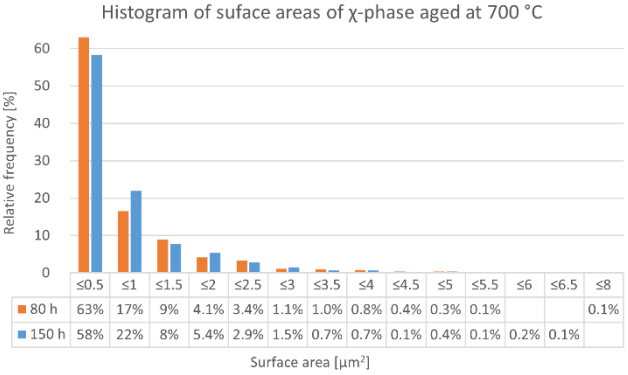

	≤0.5	≤1	≤1.5	≤2	≤2.5	≤3	≤3.5	≤4	≤4.5	≤5	≤5.5	≤6	≤6.5	≤8
80 h	63%	17%	9%	4.1%	3.4%	1.1%	1.0%	0.8%	0.4%	0.3%	0.1%			0.1%
150 h	58%	22%	8%	5.4%	2.9%	1.5%	0.7%	0.7%	0.1%	0.4%	0.1%	0.2%	0.1%	

Fig. 4. Histogram of the surface area of χ-phase after ageing at 700 °C at different times in Gr 4A steel

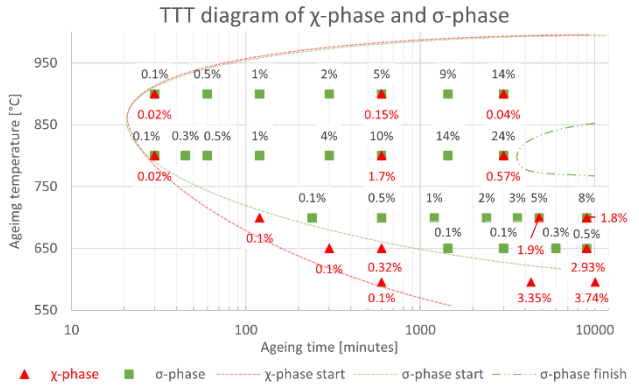

Fig. 5. TTT diagram of χ-phase and σ-phase precipitates of cast duplex steel Gr4A

4.1. Evaluation of continuous cooling

Samples for this phase are taken from the second trial. The samples were taken from Y blocks with wall thicknesses of 25, 50, 75 and 100 mm, representing different cooling rates. The cooling rates were respectively 9.5, 5.8, 4.6 and 3.8 °C/min during the studied period from 1000 to 650 °C. To evaluate the properties, the

structure was in the as-cast condition without solution annealing. Solution annealing was performed to verify the mechanical properties because DSS is usually delivered after solution annealing. Tensile and Charpy impact tests were carried out to analyse the mechanical properties. The tensile test specimens were made according to DIN 50125, shape B 10 × 50 mm. The specimens for the Charpy impact test were made according to EN ISO 148 1, 10 × 10 × 55 mm with V notch, the given results are the average of 3 tests. Results are shown in Table 4 and in Fig. 6 as a function of the cooling rate. The as-annealed condition is slightly better than the as-cast condition in yield strength and more than 4 times better in impact energy. One specimen of Y 25 failed in elongation, other properties safely met the requirements given by the standard ASTM A890. The impact energy is dependent on the cooling rate compared to the other properties.

Table 4.
Mechanical properties of the as-annealed and as-cast condition of cast duplex steel ASTM A890 Gr4A

Condition	Wall thickness [mm]	Yield strength [MPa]	Ultimate strength [MPa]	Elongation [%]	Impact energy [J]
Standard (min)	-	415	620	25	-
As-annealed	100	490	669	28.5	189.9
		484	666	31.8	
As-cast	25	465	693	25.4	57.1
		451	668	16.7	
	50	448	697	32.2	54.6
		444	681	29.8	
	75	462	699	32.7	53.2
		445	684	26.0	
	100	441	687	32.7	43.9
		444	687	26.3	

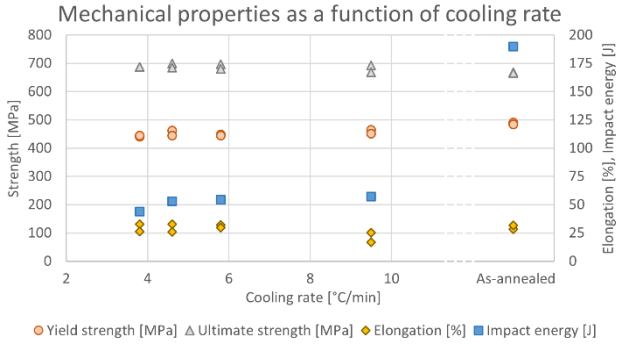

Fig. 6. Mechanical properties as a function of cooling rate of cast duplex steel Gr4A

The microstructures of the as-cast condition were analysed and the precipitates look like a fine σ-phase with coral morphology and the largest representatives are in Fig. 7. The content of all precipitates in the samples was <0.1, 0.15, 0.17 and 0.25 % with increasing wall thickness. The CCT curves of each casting were plotted on the TTT diagram in Fig. 8, where the origin of the cooling curve was experimentally plotted at 1000 °C.

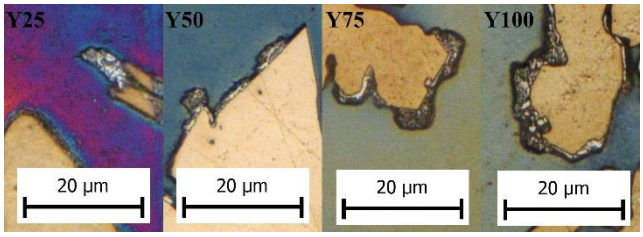

Fig. 7. Microstructure of as-cast specimens taken from Y blocks 25, 50, 75 and 100 mm of cast duplex steel Gr4A (magn. 1000x)

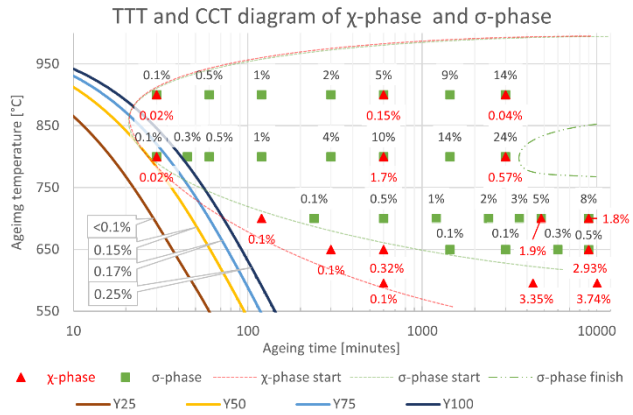

Fig. 8. TTT and CCT diagram of χ-phase and σ-phase precipitates of cast duplex steel Gr4A

5. Results discussion

This study is very important due to its foundry character because it examines the DSS in the cast state and points out the problems that arise when casting such challenging materials and indicates where research can continue. The precipitation rate during continuous cooling for the Gr4A steel used in this study was higher than in the wrought DSS in the study [16]. During isothermal heat treatment, the precipitation in the cast Gr 4A steel used in this study was slower than that of the study [12]. The TTT diagram of the study [17] corresponded most closely, but the precipitation of the σ-phase proceeded more slowly for the cast Gr4A steel used in this study. The above-mentioned studies used DSS with similar chemical composition compared to the cast Gr4A steel used in this study. The studies on precipitation rates show that there are big differences whether the DSS is in the cast condition or in the wrought condition.

6. Conclusions

- The obtained results of cast DSS Gr4A revealed the highest share of the χ-phase in the material aged at 595 °C and the highest share of the σ-phase in the material aged at 800 °C.
- Based on the obtained data, a combined TTT diagram of the σ-phase and the χ-phase, supplemented by CCT curves of a

continuously (naturally) cooled casting in a mould with different wall thicknesses was created.

- The tests showed that a wall thickness of 100 mm and a cooling rate of 3.8 °C did not lead to a significant loss of mechanical properties, as all mechanical properties safely met the requirements of the standard.
- However, the impact energy is reduced more than 4 times to 43.9 J compared to the as-annealed condition 189.9 J.
- The results published in this paper can be used to improve thermodynamic and kinetic calculations of precipitation in DSS castings. The obtained TTT and CCT diagrams can be used to predict the behaviour of real castings. The diagrams can be further extended.

Acknowledgement

This work was supported by the specific research project of BUT FME Brno, no. FSI-S-22-8015 Research in melting and metallurgical processing of high-temperature alloys.

References

[1] Knyazeva, M. & Pohl, M. (2013). Duplex steels: part I. *Metallography, Microstructure, and Analysis.* 2(2), 113-121. https://doi.org/10.1007/s13632-013-0066-8.

[2] Speidel, H.J.C. & Speidel, M.O. (2004). Nickel and chromium-based high nitrogen alloys. *Materials and Manufacturing Processes.* 190(1), 95-109. https://doi.org/10.1081/AMP-120027518.

[3] Kaňa, V., Pernica, V., Zadera, A. & Krutiš, V. (2019). Comparison of Methods for Determining the Ferrite Content in Duplex Cast Steels. *Archives of Foundry Engineering.* 19(2), 85-90. https://doi.org/10.24425/afe.2019.127121.

[4] Alvarez-Armas, I., Degallaix-Moreuil, S. (2009). Duplex stainless steels.

[5] Kim, Y. J., Kim, S. W., Kim, H. B., Park, C. N., Choi, Y. I., & Park, C. J. (2019). Effects of the precipitation of secondary phases on the erosion-corrosion of 25% Cr duplex stainless steel. *Corrosion Science.* 152, 202-210. https://doi.org/10.1016/j.corsci.2019.03.006.

[6] Müller, P., Pernica, V. & Kaňa, V. (2022). Corrosion Resistance of Cast Duplex Steels. *Archives of Foundry Engineering.* 22(3), 5-10. https://doi.org/10.24425/afe.2022.140230.

[7] Cho, H. & Lee, K. (2013). Effect of cold working and isothermal aging on the precipitation of sigma phase in 2205 duplex stainless steel. *Materials Characterization.* 75, 29-34. https://doi.org/10.1016/j.matchar.2012.10.006.

[8] Brodziak-Hyska, A., Stradomski, Z. & Kolan, C. (2014). Kinetics of the σ phase precipitation in respect of erosion-corrosion wear of duplex cast steel. *Archives of Foundry Engineering.* 14(1), 17-20. https://doi.org/10.2478/afe-2014-0004.

[9] Fargas, G., Mestra, A. & Mateo, A. (2013). Effect of sigma phase on the wear behavior of a super duplex stainless steel. *Wear.* 303(1-2), 584-590. https://doi.org/10.1016/j.wear.2013.04.010.

[10] Hosseini, V., Karlsson, L., Engelberg, D. & Wessman, S. (2018). Time-temperature-precipitation and property diagrams for super duplex stainless steel weld metals. *Welding in the World.* 62(3), 517-533. https://doi.org/10.1007/s40194-018-0548-z.

[11] Magnabosco, R. (2009). Kinetics of sigma phase formation in a Duplex Stainless Steel. *Materials Research.* 12(3), 321-327. https://doi.org/10.1590/S1516-14392009000300012.

[12] Magnabosco, R., da Costa Morais, L. & dos Santos, D. (2019). Use of composition profiles near sigma phase for assessment of localized corrosion resistance in a duplex stainless steel. *Calphad.* 64, 126-130. https://doi.org/10.1016/j.calphad.2018.12.004.

[13] Stradomski, G., Nadolski, M., Zyska, A., Kania, B. & Rydz, D. (2019). Physical and Numerical Modeling of Duplex Cast Steel Thin-Walled Castings. *Archives of Metallurgy and Materials*, 64(4), 1449-1456. https://doi.org/10.24425/amm.2019.130112.

[14] Akisanya, A., Obi, U. & Renton, N. (2012). Effect of ageing on phase evolution and mechanical properties of a high tungsten super-duplex stainless steel. *Materials Science and Engineering: A*, 535, 281-289. https://doi.org/10.1016/j.msea.2011.12.087.

[15] Fujii, K. & Fukuya, K. (2013). Effects of radiation on spinodal decomposition of ferrite in duplex stainless steel. *Journal of Nuclear Materials.* 440(1-3), 612-616. https://doi.org/10.1016/j.jnucmat.2013.04.072.

[16] Oh, Y., Yang., W.J., Lee, J.H., Kim, D.H., Yoo, W.D. & Lee, J.H. (2013). Effect of Cooling Rate on Microstructural and Mechanical Properties of SAF 2205 Duplex Stainless Steel. *Journal of the Korean Society for Heat Treatment*. 26(1), 14-20. https://doi.org/10.12656/JKSHT.2013.26.1.14.

[17] Elmer, J., Palmer, T. & Specht, E. (2007). Direct observations of sigma phase formation in duplex stainless steels using in-situ synchrotron X-Ray diffraction. *Metallurgical and Materials Transactions A.* 38(3), 464-475. https://doi.org/10.1007/s11661-006-9076-3.

[18] Gunn, R. (1997). *Duplex stainless steels: microstructure, properties and applications*. Abington Publishing.

[19] Kim, Y., Ugurlu, O., Jiang, C., Gleeson, B. & Chumbley, L.S. (2007). Microstructural Evolution of Secondary Phases in the Cast Duplex Stainless Steels CD3MN and CD3MWCuN. *Metallurgical and Materials Transactions A.* 38(2), 203-211. https://doi.org/10.1007/s11661-006-9049-6.

[20] Sousa, R. et al. (2019). On the precipitation of sigma and Chi phases in a cast super duplex stainless steel. *Metallurgical and Materials Transactions A.* 50(10), 4758-4778. https://doi.org/10.1007/s11661-019-05396-6.

[21] Padiham, A. (2007). Stainless steels heat treatment (Chapter 12). In *Steel Heat Treatment Handbook* (Second Edition, pp. 695-739).

[22] Pohl, M., Storz O. & Glogowski T. (2007). Effect of intermetallic precipitations on the properties of duplex stainless steel. *Materials Characterization.* 58(1), 65-71. https://doi.org/10.1016/j.matchar.2006.03.015.